Scripta Materialia 159 (2019) 51–57

Contents lists available at ScienceDirect

Scripta Materialia

journal homepage: www.elsevier.com/locate/scriptamat

Regular article

Novel high strength titanium-titanium composites produced using field-assisted sintering technology (FAST)

E.L. Calvert[a,*,1], A.J. Knowles[b,1], J.J. Pope[a], D. Dye[b], M. Jackson[a]

[a] Department of Materials Science and Engineering, The University of Sheffield, Mappin Street, Sheffield S1 3JD, UK
[b] Department of Materials, Royal School of Mines, Imperial College London, Prince Consort Road, London SW7 2BP, UK

ARTICLE INFO

Article history:
Received 25 July 2018
Received in revised form 17 August 2018
Accepted 19 August 2018
Available online 13 September 2018

Keywords:
Titanium alloys
Metal matrix composite
Spark plasma sintering
Phase transformations
Omega

ABSTRACT

To increase the strength of titanium alloys beyond that achievable with α-β microstructures, alternative reinforcing methods are necessary. Here, field-assisted sintering technology (FAST) has been used to produce a novel Ti-5Al-5Mo-5V-3Cr (Ti-5553) metal-matrix-composite (MMC) reinforced with 0-25 wt.% of a ~2 GPa yield strength TiFeMo alloy strengthened by ordered body-centred cubic intermetallic and ω phases. The interdiffusion region between Ti-5553 and TiFeMo particles was studied by modelling, electron microscopy, and nanoindentation to examine the effect of graded composition on mechanical properties and formation of α, intermetallic, and ω phases, which resulted in a >200 MPa strengthening benefit over unreinforced Ti-5553.

© 2018 Acta Materialia Inc. Published by Elsevier Ltd. All rights reserved. This is an open access article under the CC BY-NC-ND license (http://creativecommons.org/licenses/by-nc-nd/4.0/).

High strength, heavily alloyed titanium alloys such as Ti-5Al-5Mo-5V-3Cr (Ti-5553) can possess yield strengths of ~1300 MPa, which given the relatively low density of Ti, results in favourable combinations of specific strength (~280 kNm kg^{-1}) and specific toughness (~9 kNm$^{3/2}$ kg^{-1}) [1] compared to even the best steels, such as A300 M (267 kNm kg^{-1} and 9 kNm$^{3/2}$ kg^{-1}) [2,3]. This leads to their use for high integrity, weight critical structures such as the landing gear of twin-aisle commercial aircraft, which can account for as much as 10 % of airframe weight; this is a significant consideration in terms of fuel efficiency and therefore the emissions associated with air travel.

These alloys achieve these strengths and toughnesses through the precipitation of a high volume fraction of 10–25 nm fine scale *hcp* α phase within the *bcc* β matrix [4,5], but the improvement in properties achieved in Ti alloys has begun to plateau in recent years, following much progress that was achieved in the 1950s to 1970s [6]. Long-fibre ceramic reinforcement, e.g. with SiC has long been proposed, chiefly using relatively conventional alloys such as Ti-6Al-4V as the matrix [7], and more recently the use of high strength Ti-5553 as the matrix has achieved specific strengths as high as 2050 MPa (in tension) and 3500 MPa (in compression) [8]. However,

Table 1
Chemical analysis of Ti-5Al-5Mo-5V-3Cr gas atomised powder, and TiFeMo alloy powder (wt.%).

	Al	Cr	Fe	Mo	Ni	V	Ti
Ti-5553	5.1	2.7	0.4	5.1	0.1	5.2	80.8
TiFeMo	0	0	15.8	36.6	0	0	47.6

Table 2
Particle size distribution (PSD) of spherical Ti-5553 powder, and angular TiFeMo powder (for both the Ti-5553–10 wt.% TiFeMo and Ti-5553–25 wt.% TiFeMo composites) (μm).

	Dx10	Dx50	Dx90
Ti-5553	22	63	115
10 wt.% TiFeMo	16	40	158
25 wt.% TiFeMo	14	35	63

* Corresponding author.
E-mail address: e.l.calvert@sheffield.ac.uk (E.L. Calvert).
[1] These authors contributed equally to the work.

https://doi.org/10.1016/j.scriptamat.2018.08.036
1359-6462/ © 2018 Acta Materialia Inc. Published by Elsevier Ltd. All rights reserved. This is an open access article under the CC BY-NC-ND license (http://creativecommons.org/licenses/by-nc-nd/4.0/).

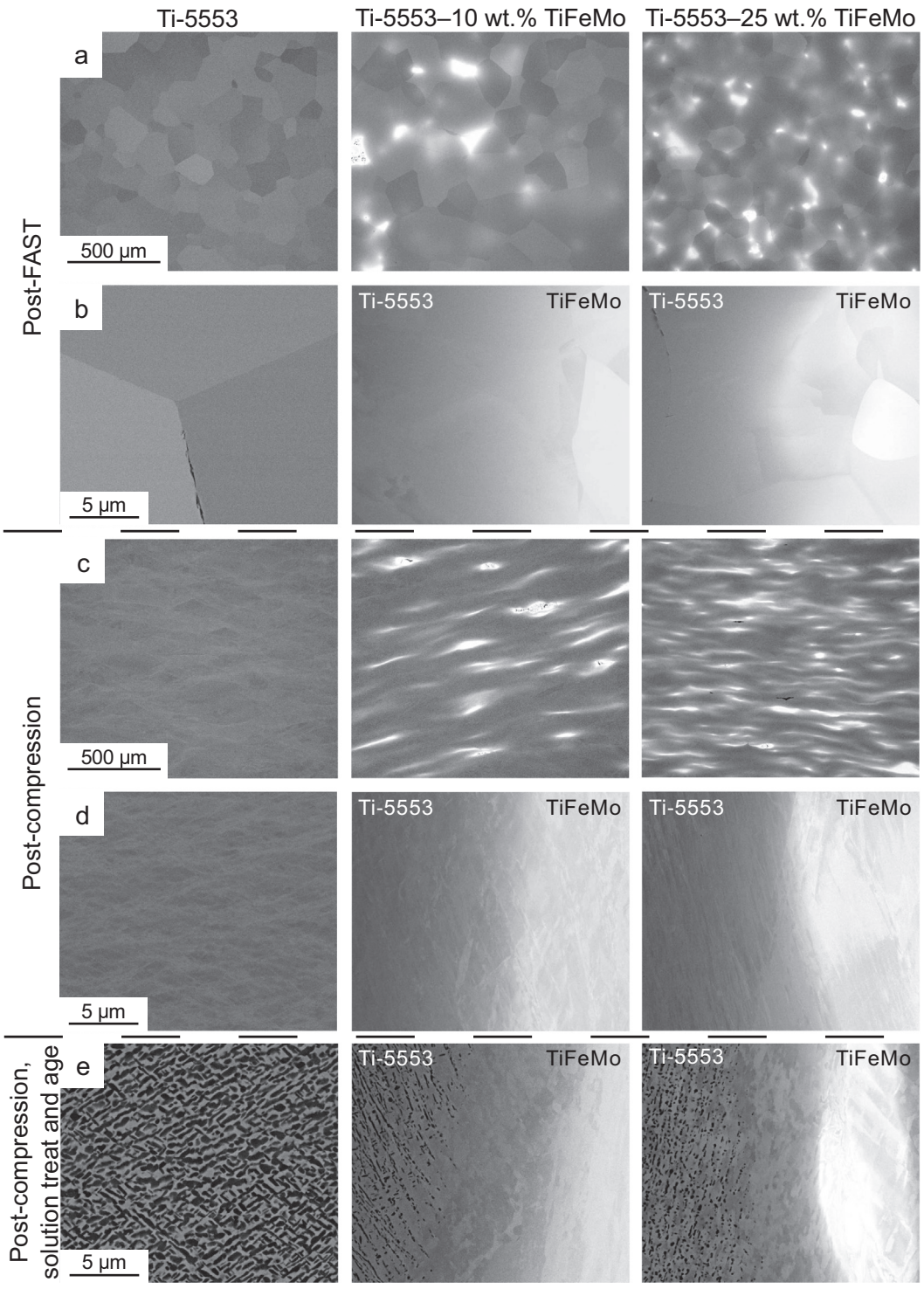

Fig. 1. Low magnification micrographs of Ti-5553 (30 min dwell) and Ti-5553–TiFeMo composites: (a) post-FAST and (c) post-compression. High magnification micrographs of Ti-5553 (30 min dwell) and Ti-5553–TiFeMo composites: (b) post-FAST; (d) post-compression; and (e) post-compression, solution treat and age.

such microstructures require the laying-up of a composite structure using ceramic fibres, which is a costly manufacturing route.

Recently, progress has been made in the development of so-called '*bcc* superalloys', which in the titanium alloy system can be realised using ~50 nm ordered β' B2 intermetallics such as TiFe in a *bcc* β A2 Ti, Mo matrix [9]. Such TiFeMo alloys can possess strengths in the order of 2 GPa, but are brittle.

Powder manufacturing of Ti components has long possessed the possibility to realise substantial cost savings through a reduction in the processing steps and machining requirements of ingot

Table 3
Mean grain size of Ti-5553 (30 and 60 min FAST dwell) and Ti-5553–TiFeMo composites (60 min dwell) (μm).

Ti-5553 30 min	Ti-5553 60 min	Ti-5553–10 wt.% TiFeMo	Ti-5553–25 wt.% TiFeMo
125 ± 10	174 ± 33	177 ± 33	117 ± 10

metallurgy [10,11,12]. In particular, field-assisted sintering technology (FAST) offers the prospect of the rapid high temperature and low cost consolidation of Ti alloy powders [13,14]. A final forging step is often found to further improve properties through recrystallisation and the break-up of α at prior-β boundaries [5]. FAST, and subsequent single step forging (FAST-*forge*), of Ti-6Al-4 V and Ti-5553 has been successfully demonstrated at both the small- and industrial-scale, and has been shown to produce microstructures similar to that of conventional material [15,16,17].

These factors lead to the following alluring concept: is it possible to produce a low cost intermetallic reinforced metal-metal composite? In the present example, should the $\beta - \beta'$ Ti powder grains be sufficiently fine in lengthscale, they might be able to accommodate plastic deformation, whilst providing reinforcement of the $\alpha - \beta$ Ti matrix. Since both materials possess a β matrix, interdiffusion offers the prospect of strong interfacial bonding without the precipitation of undesirable brittle phases [18]. In this paper, we explore FAST as a low cost processing route for the production of a Ti-5553–TiFeMo composite and evaluate its mechanical behaviour.

Wrought Ti-5553 was gas atomised to produce spherodised powder with chemistry and particle size distribution (PSD) reported in Tables 1 and 2. The TiFeMo alloy from [19] was mechanically ground to produce an angular powder, Tables 1 and 2. PSD for Ti-5553 powder was measured using a Malvern Mastersizer 3000 laser particle size analyser using the dry dispersion method; for the TiFeMo powder particles were measured post-FAST using ImageJ image analysis software [20] and a cumulative frequency distribution gave values for Dx10, Dx50 and Dx90 (Dx10 is the size of powder particles relating to 10 % of the cumulative mass, etc.).

FAST was performed using an FCT Systeme GmbH HP D 25 Spark Plasma Sintering furnace to produce three 20 mm diameter specimens; (1) Ti-5553, (2) Ti-5553 with 10 wt.% TiFeMo (Ti-5553–10 wt.% TiFeMo), and (3) Ti-5553–25 wt.% TiFeMo. For Ti-5553, a 1200°C dwell temperature was used with 30 and 60 min dwell times, whilst 60 min was used for the Ti-5553–TiFeMo composites. 35 MPa pressure, 200°C/min heating and ~250°C/min cooling rates were employed.

Two 6 mm diameter, 9 mm high cylindrical specimens were then wire electrical discharge machined from the Ti-5553 (30 min dwell) and Ti-5553–25 wt.% TiFeMo FAST specimens. They were compressed at room temperature (RT), at 0.1 s^{-1} to a true strain of 0.5 using a Servotest Thermomechanical Compression (TMC) machine [13], in order to simulate upset forging (FAST-*forge*). Two cylindrical specimens were also compressed from the Ti-5553–10 wt.% TiFeMo FAST composite, for microstructural examination. The compressed specimens were then solution heat treated at 785°C for 2 h, furnace cooled to RT, and aged at 500°C for 8 h (furnace cooled to RT) in an Elite vacuum furnace.

Specimens were sectioned parallel to the compression direction and metallurgically prepared [17]. Backscatter electron imaging (BSEI) using an FEI Inspect F50 scanning electron microscope was performed, with 10 kV accelerating voltage and ~10 mm working distance. SEM-EDX (Energy-Dispersive X-Ray Spectroscopy) line point scans across the interdiffusion regions of the post-FAST and post-aged Ti-5553–25 wt.% TiFeMo composites were performed using a Philips XL30 FEG SEM, with an Oxford Instruments detector. DICTRA Thermo-Calc 2017b, employing the TTTI3 and MOBTi1 databases [21], was used to model the diffusion in the post-FAST Ti-5553–25 wt.% TiFeMo composite across the interdiffusion region during the 60 min dwell period at 1200°C.

An FEI Quanta 200 3D SEM with a focussed ion beam (FIB) was used to mill a ~25 μm long TEM lamella, ~100 nm thick, across an interdiffused particle-matrix region of the post-aged Ti-5553–25 wt.% TiFeMo composite [22]. An SEM-EDX line point scan of the area adjacent to the TEM lamella was performed as previously, to ensure comparability with the other SEM-EDX results. Transmission electron microscopy (TEM) was performed using a JEOL JEM-2100F at 200 kV: selected area diffraction patterns (SADPs) with an aperture of 200 nm were taken from the Ti-5553, interdiffusion, and TiFeMo regions. A STEM-EDX map was performed on the Ti-5553 region of the TEM lamella.

Microhardness testing was performed using a Struers DuraScan-70 G5 with a Vickers indenter and 4.905 N load, held for 15 s, averaging ~50 measurements. For nanohardness, a Bruker Hysitron

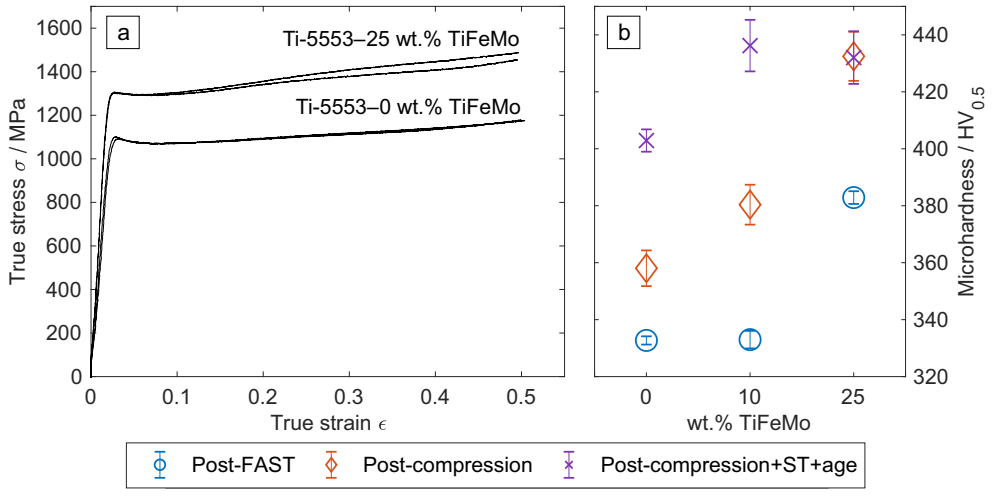

Fig. 2. Mechanical properties: (a) Flow stresses of Ti-5553 (i.e. 0 wt.% TiFeMo, 30 min dwell) and Ti-5553–25 wt.% TiFeMo compressed specimens, and (b) microhardness for all compositions and conditions: post-FAST; post-compression; and post-compression, solution treat and age.

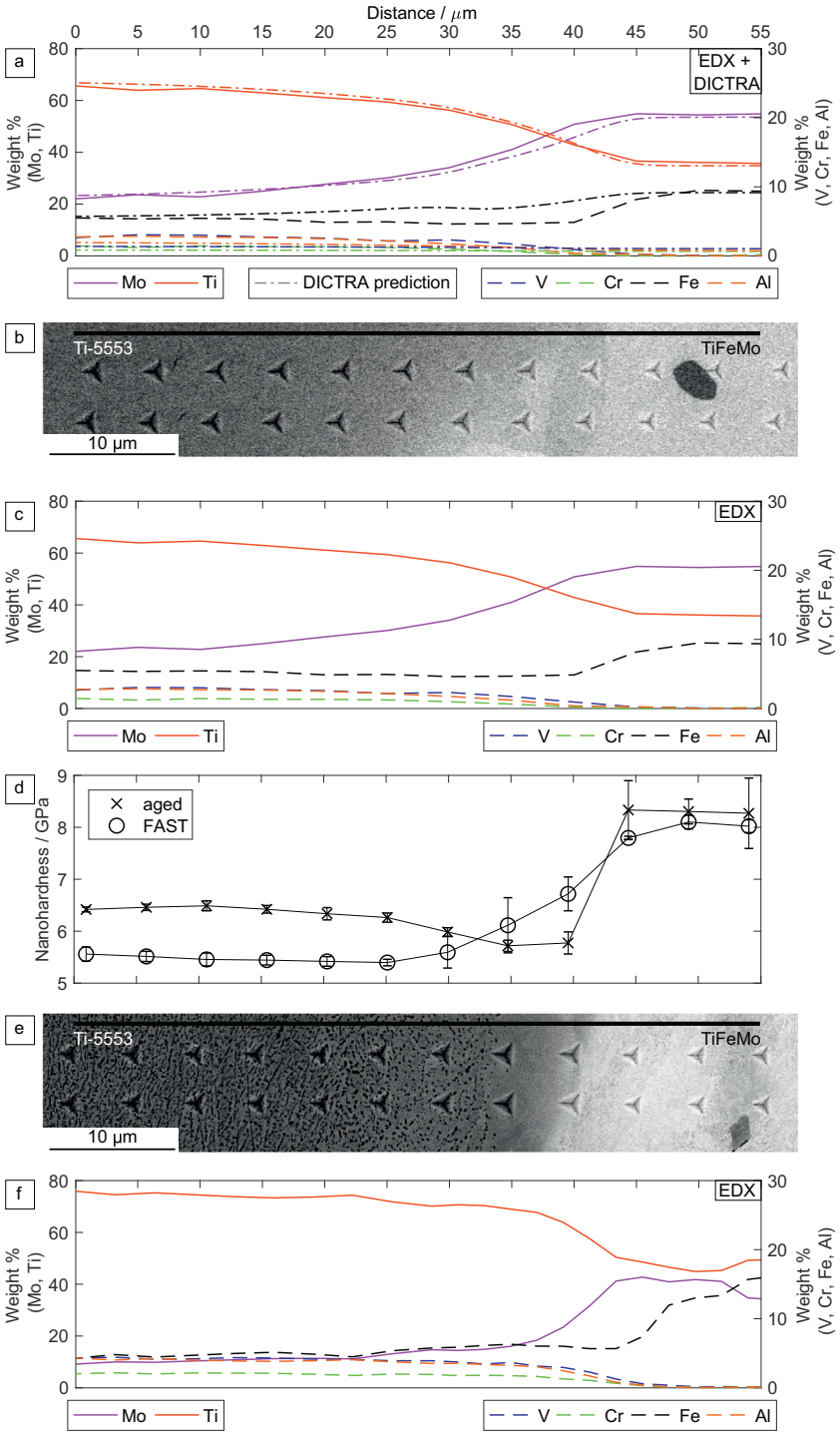

Fig. 3. Interdiffusion region of Ti-5553–25 wt.% TiFeMo post-FAST composite: (a) DICTRA thermodynamic prediction with SEM-EDX line point scan, (b) BSEI micrograph, and (c) associated SEM-EDX line point scan. (d) Nanohardness for both Ti-5553–25 wt.% TiFeMo post-FAST and post-aged composites, corresponding to indents shown in (b) and (e). Interdiffusion region of Ti-5553–25 wt.% TiFeMo post-aged composite: (e) BSEI micrograph, and (f) associated SEM-EDX line point scan. The black lines show the location of the SEM-EDX line point scans. For all subfigures the Ti-5553 region is on the left and TiFeMo region is on the right.

TI premier nanoindenter with a Berkovitch indenter and 0.01 N load was used, averaging 3–7 measurements per position, in order to assess the hardness profiles in the Ti-5553–25 wt.% TiFeMo post-FAST and post-aged composites.

The microstructures of the Ti-5553 and Ti-5553–TiFeMo composites were characterised by SEM in the post-FAST, post-compressed, and post-compressed, solution treated and aged conditions, Fig. 1. Full diffusion bonding between the Ti-5553 and TiFeMo particles was achieved for all conditions, Fig. 1b, d, and e, and the post-FAST density was determined to be 99.64 %, using the methodology outlined in [17]. The post-FAST β grain size of the Ti-5553 specimen and Ti-5553–25 wt.% TiFeMo composite were very similar, whereas the β grain size was larger for Ti-5553–10 wt.% TiFeMo, Fig. 1a. This was due to the shorter FAST dwell time for Ti-5553; 30 min as

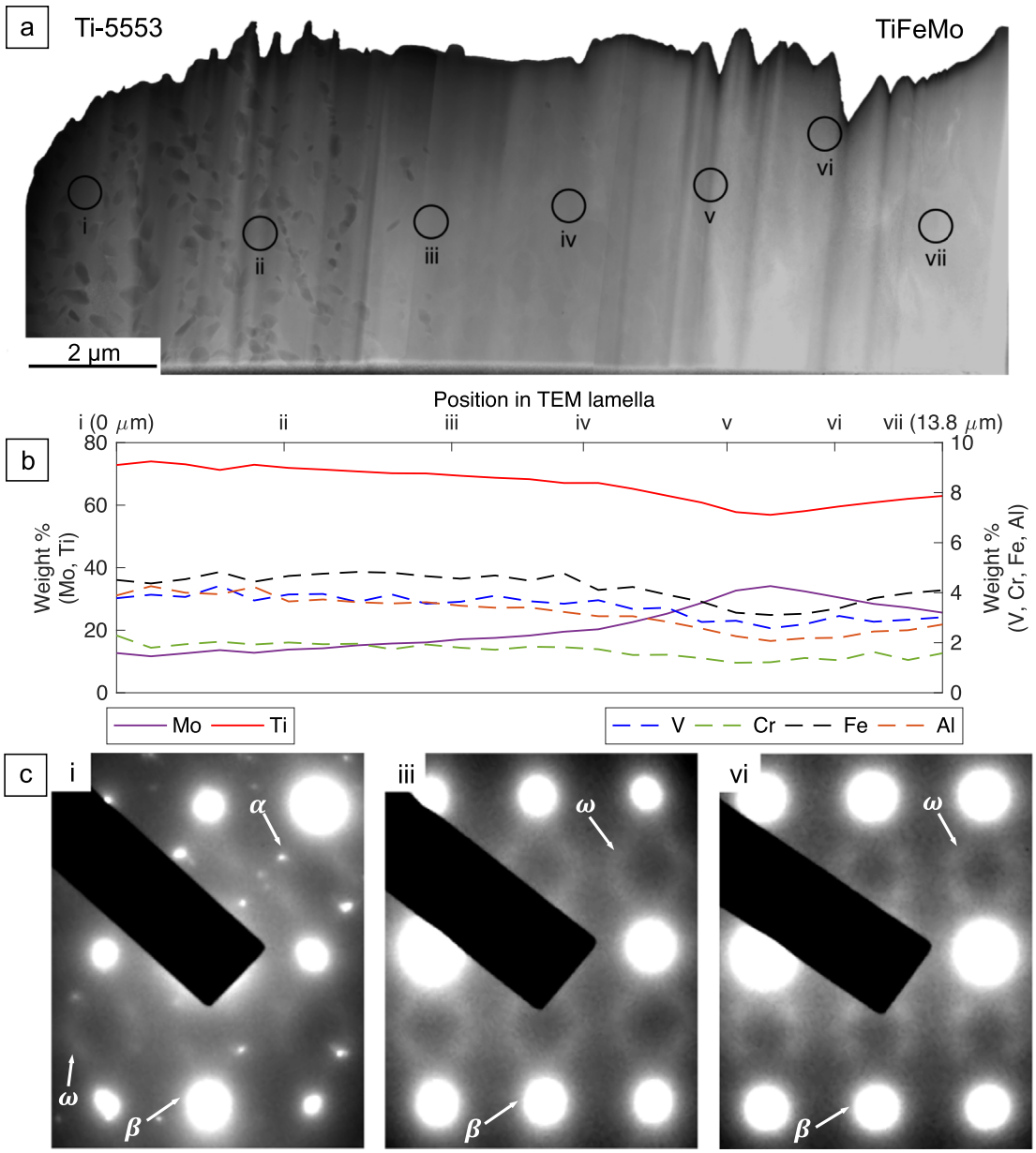

Fig. 4. TEM lamella of the interdiffusion region in the Ti-5553–25 wt.% TiFeMo post-aged composite: (a) STEM-HAADF (high-angle annular dark-field) overview, (b) SEM-EDX line point scan of the area adjacent to the TEM lamella at points i–vii, and (c) SADPs from regions; i - overlapping *bcc* β, *hcp* α, and ω reflections, iii - *bcc* β and Ti-5553/TiMo type ω reflections, and vi - *bcc* β and TiFeMo ω variant reflections ($[110]_{bcc}$ zone axis).

opposed to 60 min, and ensured that any differences in the mechanical behaviour between the Ti-5553 and Ti-5553–25 wt.% TiFeMo composite in subsequent compression testing was not due to differences in their grain sizes, Table 3. When compared to a Ti-5553 specimen produced at 60 min dwell, the Ti-5553–10 wt.% TiFeMo composite has a similar β grain size, Table 3. Therefore, the addition of 10 wt.% TiFeMo particles had limited effect on the β grain size, whereas 25 wt.% TiFeMo addition reduced the β grain size by ~1/3. This is likely due to the improved particle grinding method for the 25 wt.% TiFeMo particles, which produced smaller, more uniformly sized, and more homogeneously distributed particles within the Ti-5553 matrix, which more successfully pinned the grain boundaries [23].

In the compressed Ti-5553–10 wt.% TiFeMo composite, Fig. 1c, microcracking of the TiFeMo particles was observed; however there was an absence of cracking for particles below ~100 μm. Because of this, further refinement of the TiFeMo particle size was made for the Ti-5553–25 wt.% TiFeMo composite (Table 2), where cracking was limited to TiFeMo particles containing a high concentration of Fe-rich particles. Near the Fe-rich particles, there was also evidence of infrequent micron sized B2 TiFe intermetallics in the composites as per [9], shown in the Supplementary material. However, this was not the dominant microstructure within the TiFeMo particles, so further analysis was made on the typical particles and their interdiffusion regions. The FAST process is especially useful for processing of such Fe-rich compositions as it avoids the severe macrosegregation that can occur in Fe-rich alloys through conventional processing. This enables otherwise unfeasible alloys to be produced.

In order to evaluate the mechanical properties of the specimens, compression testing and microhardness tests were performed, Fig. 2.

The addition of 25 wt.% TiFeMo particles to Ti-5553 produced a >200 MPa increase in compressive yield strength. As the β grain size post-FAST was found to be comparable for the Ti-5553 specimen (30 min dwell) and Ti-5553–25 wt.% TiFeMo composite, this increase in strength was not due to Hall-Petch strengthening and was therefore directly attributed to the influence of the TiFeMo particles. The microhardness measurements found a general trend of increased hardness with TiFeMo particle addition, as well as with compression and ageing.

DICTRA thermodynamic modelling was used to predict the interdiffusion of elements between Ti-5553 and TiFeMo during FAST in the Ti-5553–25 wt.% TiFeMo composite, Fig. 3a. This prediction was in good agreement with an SEM-EDX line point scan performed across the interdiffusion region in the post-FAST condition, shown in Fig. 3b. Following compression, solution heat treatment and ageing, the interdiffusion profile was found to have minimal change, owing to the reduced diffusion kinetics at the relatively low solution treat and age temperatures employed, Fig. 3c and f. In particular, both Mo and Fe were seen to have diffused significantly into the prior Ti-5553 matrix, resulting in an increase in Mo and Fe compared to the nominal Ti-5553 composition, as well as a corresponding depletion of these elements in the prior TiFeMo particles. Mo and Fe diffusion resulted in reduced formation of α within the interdiffusion region, Fig. 3e, due to both stabilising the β phase [24]. The SEM-EDX line point scan of the Ti-5553–25 wt.% TiFeMo post-aged composite was performed on a TiFeMo particle containing a *bcc* + B2 TiFe microstructure, which is shown in higher resolution in the Supplementary material. These B2 TiFe intermetallics are as observed previously for TiFeMo alloys [9]. However, most TiFeMo particles appeared to be single phase A2 Ti, Mo when imaged by SEM, Fig. 1e, attributed to Fe depletion.

A substantial increase in nanohardness of ~2 GPa was observed to be strongly correlated to the Fe content in both conditions, Fig. 3d. Upon ageing, a significant increase in the nanohardness of the Mo and Fe lean prior Ti-5333 regions was achieved of 1 GPa, alongside a 0.5 GPa increase in the prior TiFeMo particles. This indicated that, despite the high nanohardness, neither B2 TiFe intermetallics nor α phase were the dominant strengthening phase in the prior TiFeMo particles and interdiffusion region.

In order to investigate the basis for the increase in nanohardness with composition, a TEM lamella was prepared across the interdiffusion region between Ti-5553 and TiFeMo in the Ti-5553–25 wt.% TiFeMo post-aged composite, Fig. 4a. Here the diffusion of Fe and Mo from the prior TiFeMo particle into the Ti-5553 matrix could again be seen in an SEM-EDX line point scan of the area adjacent to the TEM lamella, Fig. 4b. The prior Ti-5553 region was found to contain α, as demonstrated by the SADP in Fig. 4ci, and also by STEM-EDX mapping, see Supplementary material. It was observed that increasing Mo content destabilised the formation of α, as in Fig. 3e and f.

It was anticipated that the TiFeMo particles would be reinforced by both ω phase [25] and B2 TiFe intermetallics, as observed previously [9]. However, diffusion of Fe and Mo away from the prior TiFeMo particles resulted in these regions being depleted in Fe, Fig. 4b, and so having a composition within the *bcc* β single phase field [26], which prevented the formation of the B2 TiFe intermetallic.

All β regions were found to contain ω or an ω variant phase, as shown by the SADPs in Fig. 4ci, iii, and vi [27]. ω was found to co-exist in the β phase with α in the prior Ti-5553 region, Fig. 4ci [28]. It was found that the structure changed from that of ω observed in Ti-5553 [29,4] and TiMo [30] to that of an ω variant reported for TiFe and TiFeMo alloys [9,31]. Given the nanohardness data shown in Fig. 3d, this indicated that for the heat treatment applied, the regions containing the TiFeMo ω variant had a higher nanohardness than that which existed in the prior Ti-5553 matrix.

In summary, the following conclusions are drawn. (1) Ti-5553 composites reinforced with 10–25 wt.% of a high strength TiFeMo alloy have been fabricated by field-assisted sintering technology (FAST). (2) The Ti-5553–25 wt.% TiFeMo composite demonstrated compressive yield strengths of 1300 MPa, >200 MPa more than that of unreinforced Ti-5553. The microhardness was 383 HV post-FAST, which increased by ~50 HV on compression, solution treatment, and ageing. (3) Characterisation of the interdiffusion regions between Ti-5553 and TiFeMo particles by SEM, SEM-EDX, and nanoindentation showed that increased Fe and Mo lead to an increase in the nanohardness. However, this increase in Fe and Mo destabilised the α phase formation and did not result in the formation of the B2 TiFe intermetallics. (4) TEM, STEM, and SEM-EDX were used to identify that ω or an ω variant formed throughout the post-aged Ti-5553–25 wt.% TiFeMo composite, and that the diffusion of Fe and Mo were correlated to a change in the ω structure, from that of ω phase in Ti-5553 to that of the ω variant in TiFeMo, which corresponded to an increase in nanohardness.

Acknowledgments

Funding was provided by an EPSRC Doctoral Training Account (ELC) and the Design of Alloys for Resource Efficiency (DARE) programme grant EP/L0253/1 (AJK, DD, MJ). The authors acknowledge Phil Mahoney for performing nanoindentation.

Appendix A. Supplementary data

Supplementary data to this article can be found online at https://doi.org/10.1016/j.scriptamat.2018.08.036.

References

[1] J.C. Fanning, R.R. Boyer, 10TH, World Conference on Titanium; 2003; Hamburg, Germany, Wiley-VCH, Weinheim, 2003, pp. 2643–2650.
[2] Latrobe, 300M VAC-ARC Technical Data Sheet, 2007,
[3] Smiths, BS S155 Technical Data Sheet, 2017,
[4] N. Jones, R. Dashwood, M. Jackson, D. Dye, Acta Mater. 57 (2009) 3830–3839. https://doi.org/10.1016/j.actamat.2009.04.031.
[5] J.D. Cotton, R.D. Briggs, R.R. Boyer, S. Tamirisakandala, P. Russo, N. Shchetnikov, J.C. Fanning, JOM 67 (2015) 1281–1303. https://doi.org/10.1007/s11837-015-1442-4.
[6] R. Boyer, R. Briggs, J. Mater. Eng. Perform. 14 (2005) 681–685. https://doi.org/10.1361/105994905X75448.
[7] R. Leucht, H.J. Dudek, Mater. Sci. Eng. A 188 (1994) 201–210. https://doi.org/10.1016/0921-5093(94)90373-5.
[8] K.M. Rahman, V.A. Vorontsov, S.M. Flitcroft, D. Dye, Adv. Eng. Mater. 19 (2017) 3–8. https://doi.org/10.1002/adem.201700027.
[9] A.J. Knowles, T.S. Jun, A. Bhowmik, N.G. Jones, T.B. Britton, F. Giuliani, H.J. Stone, D. Dye, Scr. Mater. 140 (2017) 71–75. https://doi.org/10.1016/j.dib.2018.01.086.
[10] P. Jones, Powder Metall. 13 (1970) 114–129.
[11] A.D. Hartman, S.J. Gerdemann, J.S. Hansen, J. Miner. Met. Mater. Soc. 50 (1998) 16–19. https://doi.org/10.1007/s11837-998-0408-1.
[12] F.H. Froes, Titanium Powder Metallurgy: Science, Technology and Applications, Butterworth-Heinemann, Oxford, 2015, pp. 1–18.
[13] N.S. Weston, M. Jackson, J. Mater. Process. Technol. 243 (2017) 335–346. https://doi.org/10.1016/j.jmatprotec.2016.12.013.
[14] M. Suárez, A. Fernández, J. Menéndez, in: B. Ertug (Ed.), Sintering Applications, InTech. 2013, pp. 319–342. https://doi.org/10.5772/53706.
[15] C. Menapace, N. Vicente, Jr, A. Molinari, Powder Metall. 56 (2013) 102–110. https://doi.org/10.1179/1743290112Y.0000000003.
[16] N.S. Weston, F. Derguti, A. Tudball, M. Jackson, J. Mater. Sci. 50 (2015) 4860–4878. https://doi.org/10.1007/s10853-015-9029-6.
[17] E.L. Calvert, B. Wynne, N.S. Weston, A. Tudball, M. Jackson, J. Mater. Process. Technol. 254 (2018) https://doi.org/10.1016/j.jmatprotec.2017.11.035.
[18] D. Poddar, Int. J. Recent Trends Eng. 1 (2009) 93–99.
[19] A.J. Knowles, N.G. Jones, O.M.D.M. Messé, J.S. Barnard, C.N. Jones, H.J. Stone, Int. J. Refract. Met. Hard Mater. 60 (2016) 160–168. https://doi.org/10.1016/j.ijrmhm.2016.07.008.
[20] W. Rasband, ImageJ 1.46r Image Analysis Software, 1997.
[21] J. Andersson, T. Helander, L. Höglund, P. Shi, B. Sundman, Calphad 26 (2002) 273–312.
[22] D. Tomus, H.P. Ng, In situ lift-out dedicated techniques using FIB-SEM system for TEM specimen preparation, Micron 44 (2013) 115–119. https://doi.org/10.1016/j.micron.2012.05.006.
[23] F.J. Humphreys, M.G. Ardakani, Acta Mater. 44 (1996) 2717–2727. https://doi.org/10.1016/1359-6454(95)00421-1.

[24] G. Lütjering, J. Williams, in: B. Derby (Ed.), Titanium, Springer-Verlag Berlin Heidelberg, Berlin, 2007, pp. 283–336. https://doi.org/10.1007/978-3-540-73036-1.
[25] S.K. Sikka, Y.K. Vohra, R. Chidambaram, Prog. Mater. Sci. 27 (3) (1982) 245–310. https://doi.org/10.1016/0079-6425(82)90002-0.
[26] A.J. Knowles, N.G. Jones, C.N. Jones, H.J. Stone, Metall. Mater. Trans. A Phys. Metall. Mater. Sci. 48A (2017) 4334–4341. https://doi.org/10.1007/s11661-017-4134-6.
[27] S. Banerjee, P. Mukhopadhyay, Phase Transformations: Examples From Titanium and Zirconium Alloys, Elsevier, Oxford, 2007, pp. 475–484.
[28] Y. Zheng, R.E. Williams, H.L. Fraser, Scr. Mater. 113 (2016) 202–205. https://doi.org/10.1016/j.scriptamat.2015.10.037.
[29] S. Nag, R. Banerjee, R. Srinivasan, J.Y. Hwang, M. Harper, H.L. Fraser, Acta Mater. 57 (2009) 2136–2147. https://doi.org/10.1016/j.actamat.2009.01.007.
[30] M. Sabeena, S. Murugesan, R. Mythili, A.K. Sinha, M.N. Singh, M. Vijayalakshmi, S.K. Deb, Trans. Indian Inst. Met. 68 (2014) 1–6. https://doi.org/10.1007/s12666-014-0426-3.
[31] Y. Zheng, D. Huber, H.L. Fraser, Investigation of a nano-scale, incommensurate, modulated domain in a Ti-Fe alloy, Scr. Mater. 154 (2018) 220–224. https://doi.org/10.1016/j.scriptamat.2018.06.010.